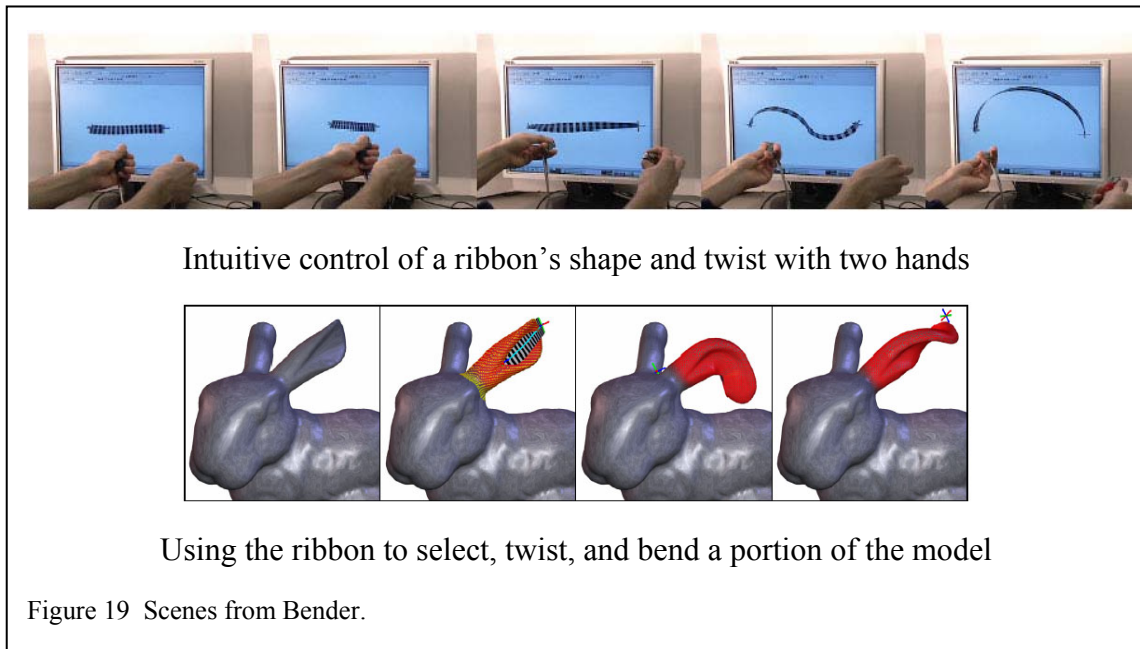


## FINDINGS

We discuss the major findings for each one of the activities listed in the Activities section

### *High Level Application Interface (Rossignac and Shaw)*

- **Bender:** (Figure 19) Two models of a ribbon have been developed. The first model is based on a **bi-arc** central wire and on a continuous interpolation of the transversal twist. The shape of the wire and the twist around it are easily controlled by the user, holding a 3D tracker in each hand. When a sufficiently-high resolution prototype of the Digital Clay becomes available, these trackers will no longer be necessary, as the physical surface will be controlled to offer the functionality of tracking the position and orientation of two coordinate systems, each defined by three finger-tips. The bi-arc is a curve in three dimension that is made of two smoothly joined circular arcs. Hence, it may have inflections (S shape). The modeling of the central wire with a bi-arc has allowed us to develop a solution to the space tearing problem that all space warp techniques face, but imposes constraints on the RoI. The second model is based on the helix defined by a screw motion interpolating the left and right-hand coordinate systems. When the helix is used as a central line for the ribbon, the user can no longer form S-shape, but may use a larger RoI, better suited for “gentle” warps. The designer has now the choice of using the Twister deformations where each hand influences the shape of the surface within its spherical RoI or of using the Bender deformations, where the RoI is a tube around a central line modeled by a bi-arc or a helix. All three approaches are intuitive and effective. Each one offers advantages for specific design needs. A report has been produced and submitted for external



publication.

- **Poker:** (Figure 20) The project explores the interpolation of a scalar or vector field over a surface. The interpolation is couched in terms of PDE, but solved directly on a triangulated representation of the surface, using the Laplace-Beltrami operator to implement the Laplacian and bi-Laplacian operators. To achieve interactive response times, a technique for localizing the solver to an interaction area has been developed. The solver has been successfully applied to several problems: (1) compute in realtime physically-plausible evolutions of the shape of the surface in response to forces applied by the user through a Phantom Haptic device, (2) smoothen a complex surface to “erase” unwanted features, and

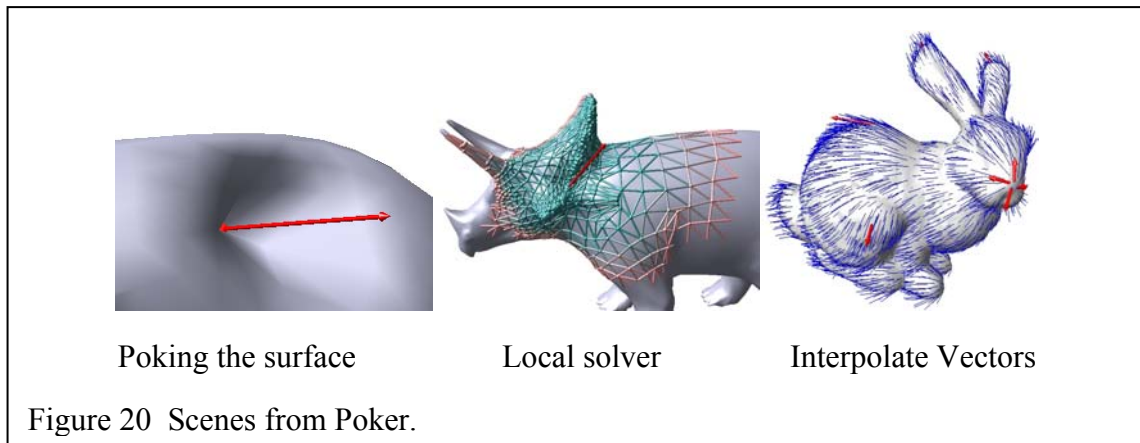


Figure 20 Scenes from Poker.

(3) the interpolation of a vector field over the surface. A report has been produced and submitted for external publication.

- Tuner:** The simulation results obtained with the software developed by Master Student Brian Whited correspond to the actual deformation of physical prototypes of the Formable Crust manufactured by PhD student Austina Nguyen using Rapid Prototyping. Hence, demonstrating the value of the simulator as a design tool for future Digital Clay applications. The discussion of the solver and its results have been incorporated in Austina Nguyen's dissertation. She has successfully defended her PhD in ME under Dr. Rosen.
- Coach:** Undergraduate students in Computer Science who have taken a course with Dr. Rossignac have been exposed to the challenges of the Digital Clay project. Several of them have requested to be involved in research projects related to the Digital Clay. Joy Shieh is one of them. Under the supervision of Dr. Rossignac, she has developed a 2D prototype for editing the trajectory of a point as it happens, in realtime. The user can play the animation several times to understand which part needs to be adjusted. Then, as the animation is played, the user may influence the trajectory of the point over a desired time interval by pushing it more or less in desired directions. The value of the paradigm has been demonstrated in a prototype system implemented by Joy Shieh for editing the curve formed by the trajectory of the moving point. The student has signed up for a second research project, aimed at extending these studies and at submitting the results for publication.
- Tritops:** As a compromise between the interface popular today (2D mouse) and the not yet available full fledged version of Digital Clay, we have developed a new concept that is best described as a mouse with 3 horns. Hence the name "tritops". Each horn is a computer-controlled piston serving as an independent input and output device. By placing a finger at the tip of each horn, the user will be able to control the position and orientation of the mouse (mobile base) and to sense and apply pressure on the pistons. PhD student (Ignacio Llamas) and Master's student (Gordon Brown) under the supervision of Dr. Rossignac have been collaborating with students and staff from ME to design and manufacture a passive prototype of the Tritops. It has been integrated equipped with passive springs and a Polyhemus tracker and has been interfaced with the Twister software for preliminary testing. The objective now is to assess its suitability for haptic rendering and force-based human-shape interaction.

## ***System Implementation and Control (Wayne Book)***

The efforts and prototyping, analyzing and experimenting with prototype digital Clay systems have revealed a number of key results which move the project toward its eventual success. The new results during the past year are summarized in the following section.

- Precise control of fluid actuators using PWM actuation is possible and suitable for digital clay.
- User applied forces can be filtered from the considerable pressure fluctuations to command the motion of the cells for purposes of shaping digital clay and for re-rendering haptic sensations.
- Position can be estimated from pressure measurements on either side of a pulse width modulated valve such that single movements of a cell would not need explicit position sensors. When no user applied forces are applied the accuracy is within 0.5%. The positioning under normal user applied force

variations remains accurate to within 1mm for travels of over 60 mm. This positioning approach requires careful calibration of the valves, however. While these calibrations are accurate in the short run, we have noticed the calibration drifts with time. Consequently it would be preferable to have some type of direct position sensing.

- Densities of cells have been obtained in row and column geometries with a spacing of 5 mm between cells. The target of 3 mm seems feasible. The technology of stationary SLA pipes with moving glass posts and sealing via O-rings appears to be viable based on preliminary tests, although other arrangements are being considered.
- Actuation of cells of density approaching the target of 3mm are feasible using current valve technology with a shared valve approach. The prototype constructed uses row control valves to trigger the opening and closing of access to one row of pistons. The access control is based on a membrane deformed by the pressure of the row control valve to block or open the access. Flow to the pistons in that row is then controlled by flow control valves, one for each piston in the row. Hence  $2N$  valves can control  $N^2$  pistons. Current construction uses SLA techniques but the layered design lends itself to other techniques.
- Sensors that can be embedded into an array of actuators have been studied theoretically and with small breadboard tests. Several techniques show promise but are not conclusive at this time.

## ***Kinematics for Shape Display (Imme Ebert-Uphoff)***

**Findings in Years 1 & 2 – Summary:** A new type of mechanism, the Formable Crust (see Figure 12 in Activities and reports of previous years), was developed and its properties were investigated. A graduate student, Paul Bosscher, successfully completed his M.S. thesis on this topic. Results were also published in 2 refereed conference papers, one journal paper (under review) and resulted in the invention of a new multi-concentric spherical joint mechanism (patent pending). Other groups of the Digital Clay project are currently working on the implementation of the Formable Crust in various forms.

**Findings in Year 3:** The main thrust of Year 3 was the investigation of the modified Bed-of-Nails architecture described in Section “Activities”, yielding the following results:

- 1) First of all, the clear advantage of this mechanism over the traditional Bed-of-Nails architecture is that it allows a greatly reduced number of actuators ( $2n+1$  instead of  $n^2$ ) to control the array of  $(nxn)$  nails. The disadvantage is that actuation cannot happen simultaneously for each nail, but only for one rows of nails, therefore increasing the time required to produce a given profile by a factor of  $n$ .
- 2) It was found that the modified Bed-of-Nails architecture shows great promise for scaling to a large number of nails. Not only does it only require  $2n$  simple binary actuators, but the actuators are all arranged along straight lines on the outside of the device, thus rendering the design manufacturable by existing mass fabrication technologies. Nevertheless, there are still several scalability issues to be solved, which are identified below.
- 3) Overall Scalability Issues Identified: Challenges pertain to both scaling *up* the number of nails and scaling *down* the geometry of the mechanism. Presently, these scalability issues have not been adequately resolved and will require further research. A total of eight challenges were identified, including potential solutions for select issues. The four most critical challenges are described below. Challenges 1&2 relate to Friction and Challenges 3&4 relate to precision/tolerance (3&4).

**Challenge 1: Net Friction Force is Proportional to Number of Nails** — Inherent to this actuation methodology is some sort of frictional latch at each nail hole in the Pushing Plate. Intuitively, the net frictional force increases proportionally as the number of nails increases. Thus, for larger arrays of nails, a stronger Pushing Plate actuator is necessary to overcome this friction. This obstacle can potentially be overcome by reducing the friction at each hole, which requires reducing the nail mass to maintain adequate support, and which is accomplished by using a friction grip sheet with either less stiffness or a lower coefficient of friction. On the other hand, decreasing size of the mechanism will reduce the amount of friction required for each pin and may thus solve this problem by itself.

Decreasing geometry also requires increased precision in the design of the friction grip to obtain an appropriate frictional force. A mechanism which uses spring-loaded ratchet rather than friction (Figure 21) may exhibit more predictable behavior, and therefore may be more scalable.

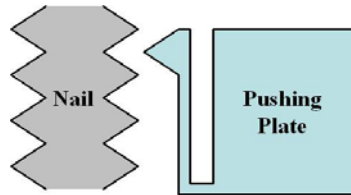


Figure21 Ratchet interface between push plate and nail.

**Challenge 2: Friction Grip Wear Increases with Number of Nails** — Wear is a problem with the current friction grip sheet design due to the constant rubbing of components. When one hole wears to the point that it can no longer support the weight of its nail, the entire sheet must be replaced. This becomes more unfeasible—and more likely to occur—for a larger number of nails. This could be alleviated by employing separate friction fittings for each hole, but this too becomes unfeasible in both manufacture and assembly as the number of nails increases. The spring-loaded design pictured in Figure 21 may help resolve this issue as well.

**Challenge 3: Tolerance Problems Increase with More Nails, Smaller Size** — The proposed design is prone to occasional binding in the slider latching mechanism when the slider hits a thread on the screw due to misalignment. This prevents the slider from being engaged, and thus prevents an entire row of nails from being locked. A similar situation occurs when the separation between two nails is not exactly equal to the hole separation in a slider, and one nail therefore becomes engaged too early, preventing others from becoming engaged. Increasing the number of nails increases the probability that these problems will occur. Furthermore, having more nails per row increases the number of nails which are affected if such a malfunction does occur. This problem can be addressed to some extent by increasing the manufacturing precision of the mechanism. However, precision actually decreases as the device is scaled down in geometry; therefore, this will become more of a problem for smaller-size mechanisms. This can perhaps be addressed by developing a more fault-tolerant latching mechanism. A new slider could also be introduced with compressible (i.e. rubber or spring-loaded) latching edges such that a misaligned edge could be compressed, allowing the other edges to latch properly.

**Challenge 4: Precise Nail Thread Shape Necessary, but Difficult on Small Scale** — For semi-continuous nails of small geometry, two problems may occur involving the thread shape and size. First, if the threads are deeply cut and close together (Figure 22a), threads can shear off due to the friction fitting in the Push Plate or the latches in the sliders. If these threads are more widely spaced (Figure 22b), the thread slope becomes more vertical, allowing the latching mechanism to slide out of the groove easily. The nail height resolution also decreases for the latter case. Both of these problems may also become worse as the device size decreases due to a decrease in manufacturing precision ability. These two problems can be alleviated by developing a truly continuous nail latching mechanism. Such a mechanism could operate by friction, electromagnetism, or other means.

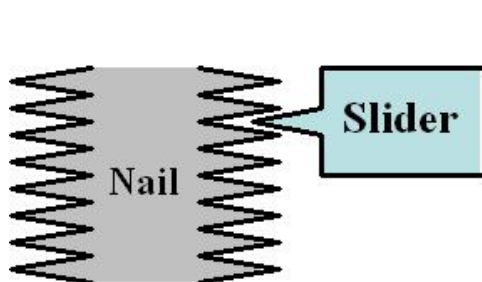


Figure 22a Deep Threads.

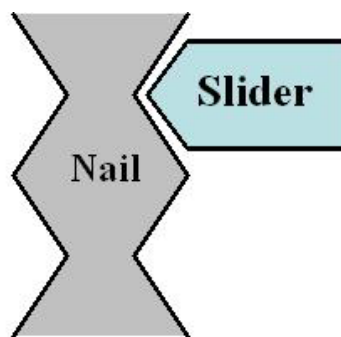


Figure 22b Shallow Threads.

## ***Design and Manufacture of Digital Clay's Kinematic Structure (David Rosen)***

**Formable Crust Design-for-Manufacture:** Designs for arrays of compliant spherical joints have been developed that can be fabricated readily using stereolithography machines. Austina implemented her math models for predicting crust shape in Matlab and conducted many computational experiments. Results show that both models predict very similar shapes in many cases, but the model of as-manufactured shapes takes much longer to solve. Results are consistent with simple hand-held experiments with physical crust models. A typical model solution is shown in Figure 23, where the heights of 5 spherical joints have been specified for a 4x6 array.

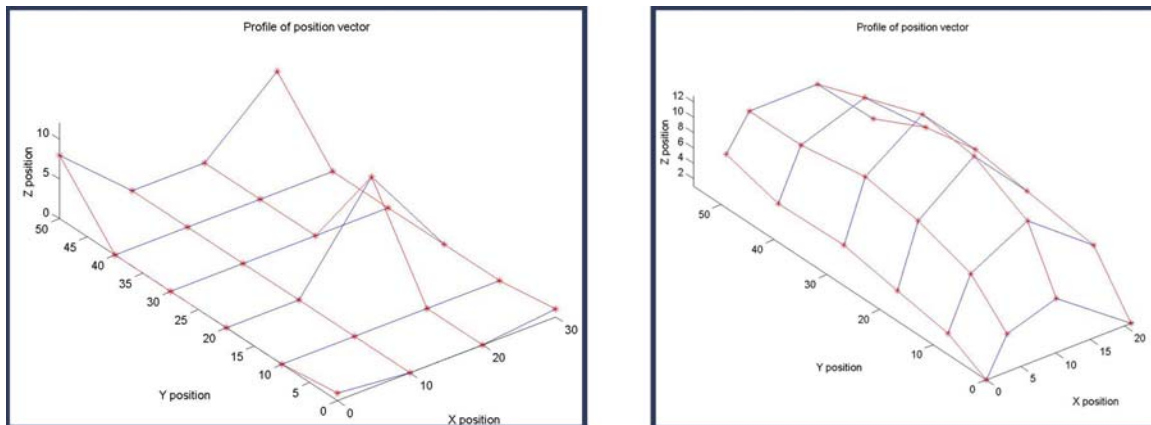


Figure 23 Surface position experiment. Inputs (Left). Results (Right)

**Topology Optimization:** The formulation of unit cell design and topology/shape optimization problems has been completed. Analysis models for 2-D unit cells have been developed that apply to both high stiffness structures and compliant structures. Extensions to 3-D are underway, as are shape and topology optimization methods.

**SL Material Properties:** Mechanical properties of two materials, SL5510 from Vantico and SOMOS 10120 from DSM, have been tested over time periods of 1 day to 3 months. Elastic modulus, yield strength, elongation at break, and fatigue life have been determined. Treatments of acetone, isopropyl alcohol, baking soda, ammonium have been investigated, in addition to control samples (no treatments). Results help us to select appropriate materials and treatments for digital clay applications, and indicate design constraints on properties as we develop new digital clay configurations and concepts.

## ***Fundamental Flow Mechanisms (Ari Glezer)***

### **Overview**

Earlier work focused on the development of a position sensing procedure in which the piston position was estimated by monitoring the volume flow rate through the feed valves. The flow rate was estimated from measurements of the pressure drop across each valve using integrated pressure sensors upstream and downstream of the valve. A triangulating laser distance measurement system determined the true position of the cylinder, and thereby enabled an assessment of the resolution and cumulative error over time. During the present reporting period, an approach for direct measurement of the absolute piston position was developed by means of a modified LVDT (which is discussed in more detail in a later section of this report). Measurements of the absolute position have virtually no cumulative errors and therefore greatly improve the repeatability of the system and allow controlled incremental corrections as well. The required hardware and software are currently being developed in order to best accomplish this task.

In addition to the development of the LVDT position measurements, the work during the present reporting period has also focused on the design of a scalable, integrated actuator module. In the earlier stages of this work the actuator was an off the shelf miniature pneumatic piston cylinder device. However, the new integrated module is fabricated using stereolithography and includes the control valves a cylinder and a piston along with the LVDT position measuring system. The new module is nominally 108 mm tall (55 mm travel) and can be packed so that the pistons center to center distance is 16.5 mm. It is anticipated that once the actuator is characterized, it will be designed with further reduction in size.

## Main Findings

During the present reporting period, a new approach was developed for position sensing using an integrated modified linear variable differential transformer (LVDT) that was calibrated and characterized using a triangulation laser-based position measurement system. The fluidic cell (shown in Figure 24) is made up of a removable face plate and a module, which houses the fluidic channels. The module houses two controllable miniature solenoid valves for the piston/cylinder actuator along with the LVDT position measuring system. This new module is 108mm tall, has a center to center distance of 16.5mm, and has a travel distance of 55mm. The underlying base plate is in fluidic communication with high and low pressure reservoirs. The LVDT consists of a glass tube, (shown in dark blue in the Figure 24), which is wrapped with magnet wire to create the primary and secondary coils. The tube is then placed within the fluidic cell by separating the module (shown in red) and the face plate (shown in light blue). The glass tube has disks at either end to create a seal between the sensor and the cell and isolates the electronics from the fluidics of the module. O-rings located on the piston and the rod endplate form dynamic seals to prevent leakage between the top and bottom cavities of the cylinder and a top seal. The integrated LVDT module drops in the housing and the lead wires protrude through the shell facilitating its connectivity.

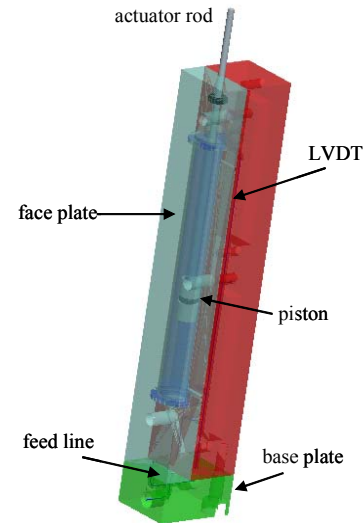


**Figure 24** Fluidic actuator cell

As noted above, in the original approach the positioning of the piston relied on measurement of the pressure drop across the valves and calculating the volume flow rate using software and thereby inferring the piston position. However, independent optical measurement of the piston position revealed that the transients associated with the opening and closing of the valves and other errors associated with the integrated pressure measurements result in cumulative position errors over time. The new LVDT approach provides a simple method for direct measurement of the absolute piston position.

Some preliminary measurements of the piston position are shown Figure 25. These traces are obtained by repeated (nominally time-periodic) piston displacements which are measured simultaneously by the LVDT and the laser positioning system. The traces (not on the same scale) show good agreement between the two independent measurements of the absolute position of the piston. The primary issue that will be resolved in the near future is improvement of the signal to noise ratio of the LVDT signal by using better, low-noise amplifiers. In these measurements, the LVDT was actuated at 7 kHz. The LVDT that is embedded in the fluidic cell has a single-layer primary coil that spans the entire length of the cylinder. It is important to note that since the LVDT is a transformer, a voltage gain can be obtained with a proportional reduction of output current and therefore a two layer secondary coil which also spans the entire length of the cylinder cavity was implemented.

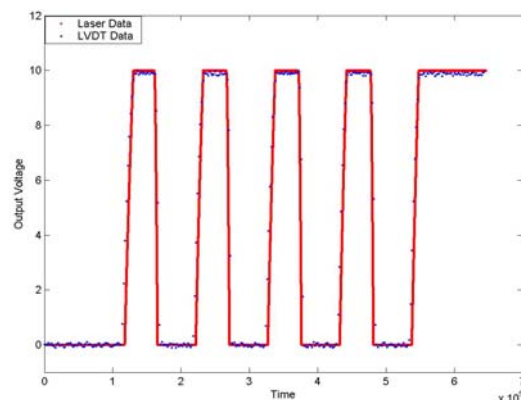


**Figure 25** LVDT and optical position measurements.

## ***MEMS Design and Fabrication (Mark Allen)***

- ***MEMS compatible fabrication of PZT stack actuators:***

As described in former report, the actuation mechanism being investigated for the micromachined hysteretic valves is based on piezoelectricity. To avoid dangerous high voltages in the device while maintaining the high electric fields necessary for PZT actuation, a parallel PZT stack structure has been designed and analyzed. It consists of multiple thin PZT pieces oriented in one plane so that they can be fabricated in a single processing step. Between each of the PZT thin pieces, there are actuation electrodes.

There are two ways to obtain the parallel-stacked PZT structure. One is to build “comb” shaped electrodes first, made from either Si or SU-8 (with be coated with Cu later), then fill PZT into the comb grooves. The other way is to construct a free standing PZT stack first, then fill the gaps with Cu by electroplating to form the electrodes. Three different fabrication methods had been investigated to fabricate the parallel PZT stack structure -- slip casting, tape casting and laser cut have been investigated as mentioned in former report.

Although all of these methods are possible, they all have various problems: time consuming (several days for each batch), higher cost, huge shrinkage (slip casting or tape casting), thermal stress & fragility (laser cutting) etc. So special expertise and higher expense are need for the experimental environments than we have now.

A quite different method has been investigated -- using traditional dicing saw. It is proved a fast, economical way. Since no high temperature process is involved, there is no thermal stress or shrinkage. Free-standing PZT stacks with tines 50um in width or larger can be made within hours without any damage. Also, it is completely MEMS compatible and can be carried out in clean room followed by standard MEMS processing to make PZT stack actuators. Figure 26 and Figure 27 are two photos of the diced PZT taken under microscope, view from top and isometric direction separately. It can be found that the cuts are quite uniform, deep (through the 1mm PZT disk) and without any burning marks or thermal stress damage.

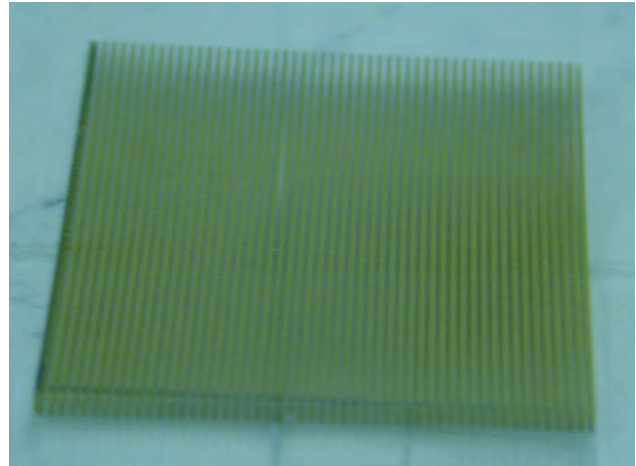
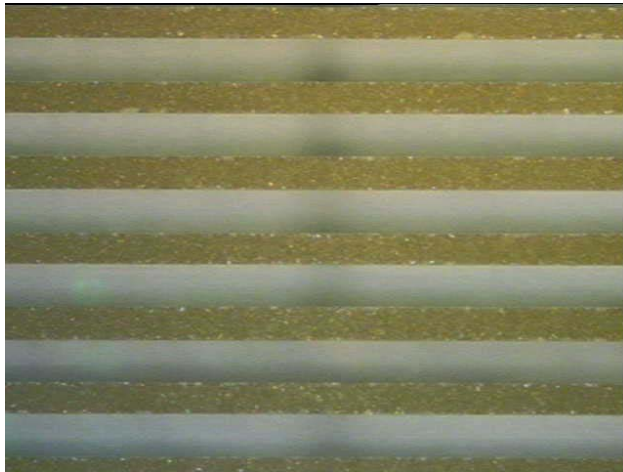


Fig 26. Microscope photo of the diced PZT, top view      Fig 27. Microscope photo of the diced PZT isometric view

A finite element model for parallel PZT stack actuators has also been developed. Static and modal simulations have been carried out and compared with the theoretical calculations. Both copper and organic (i.e., SU-8 photo definable epoxy) separations between each PZT have been modeled as suitable enclosure and elastic materials for the PZT multi-stack actuators.

Figure 28 and 29 are simulations results of the PZT stack actuators with ‘cymbal’ caps. Figure 28 shows the result using SU-8 material as separation and enclosure materials, while Figure 29 is the result of using copper. The dimensions for PZT pieces, SU-8 or Cu separations and are the same: PZT is 1.2mm long, 80um wide, SU-8 and Cu are also 80mm in width. Driving voltage is 50V for both cases. There are 8 PZT pieces in each stack actuator.

From the results, we can see that use of SU-8 as separation/enclosure materials will give a little larger deflection. There is another important advantage by using SU-8 instead of Cu -- it can save one electroplating process. This makes the whole process easier. Furthermore, it circumvents the possible damage of PZT caused in acid chemicals used in electroplating. The simulation result also shows that an about 1.2mm\*0.8mm\*1mm actuator will give a deflection of 0.6um. By increasing the driving voltage or the number of PZT pieces in the stack actuator or by reducing the width of PZT piece, we can obtain larger deflection. A couple of um deflection (the valve requirement) is possible for this type of PZT stack actuators within 3mm \* 3mm \*1mm scale fabricated by MEMS technology.

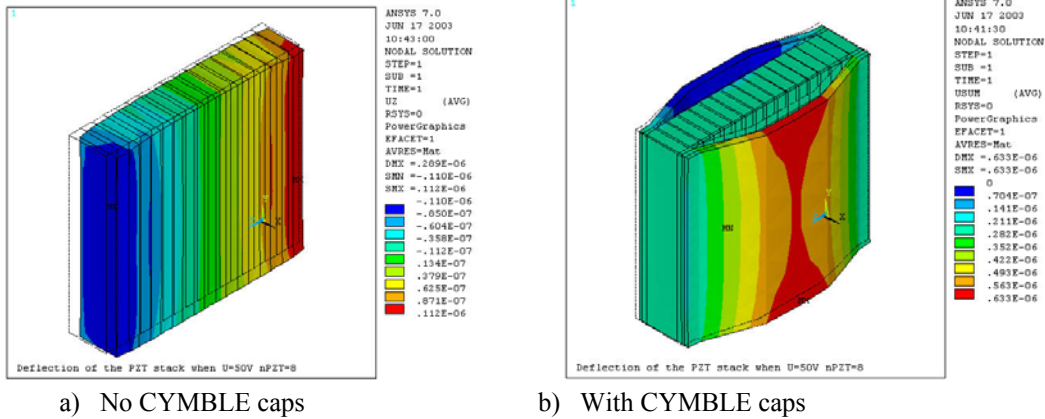


Figure 28 PZT stack actuators using SU-8 as separation/enclosure material

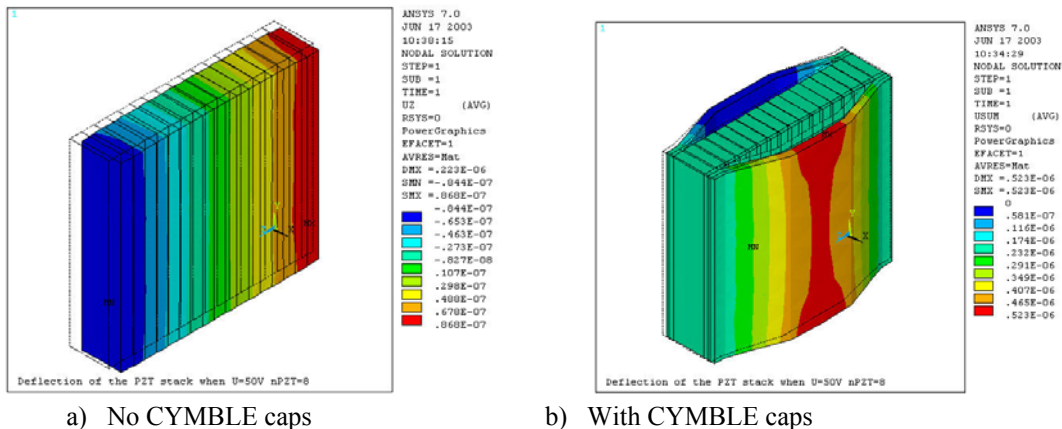
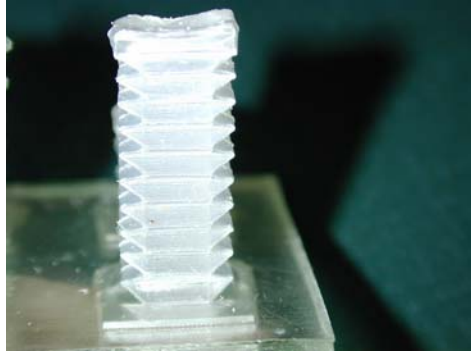


Figure 29 PZT stack actuators using Cu as separation/enclosure material

- **Fluidic cells (bubble actuators) for driving the skeleton of the clay:**

Mass-manufacturable corrugated linear and angular actuators were also investigated. Demos of linear bubble actuators of 6mm\*10mm have been designed, analyzed, fabricated and characterized. Those bubbles actuators are made by Parylene coating and have deflections of approximately 20mm – about 5mm in height when fully shrunk and up to 30mm when inflated.

Prototypes of “joints” with angular bubble actuators have also been designed, analyzed, and fabricated. Further characterization will be carried out. Figure 30 a) to d) are the photos of the linear bellows-shaped bubbles and “joints” with 3 types of angular bubble actuators separately. Among all these 4 types of bubble actuators, a), c) and d) can be scaled down to smaller than mm scale and batch fabricated by MEMS technology.



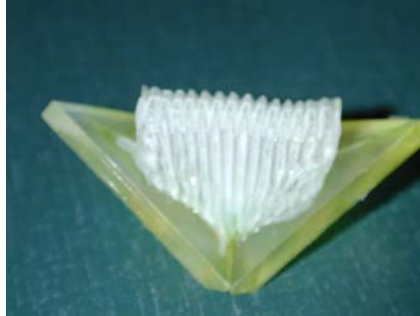
a) Linear bellows-shaped bubble



b) Lantern-shaped angular bubbles

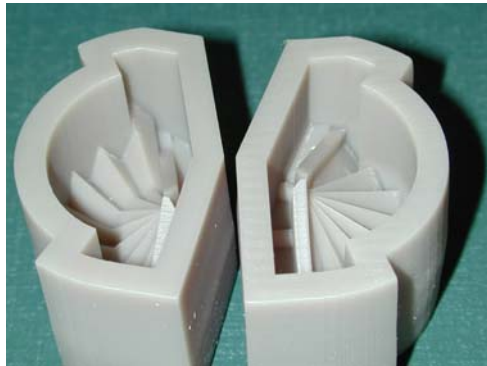


c) "Half-bellows" angular bubble



d) Declined "half-bellows" angular bubble

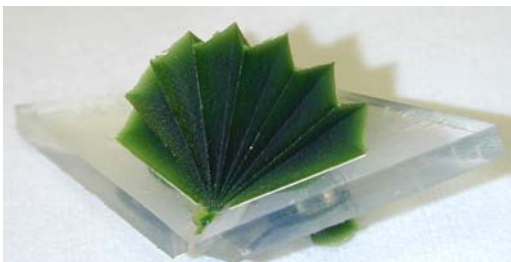
Figure 30. Prototypes of 4 types of bubble actuators



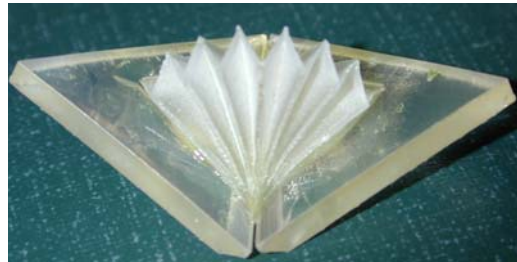
a) Corrugated mold by SLA



b) Transferred PDMS mold



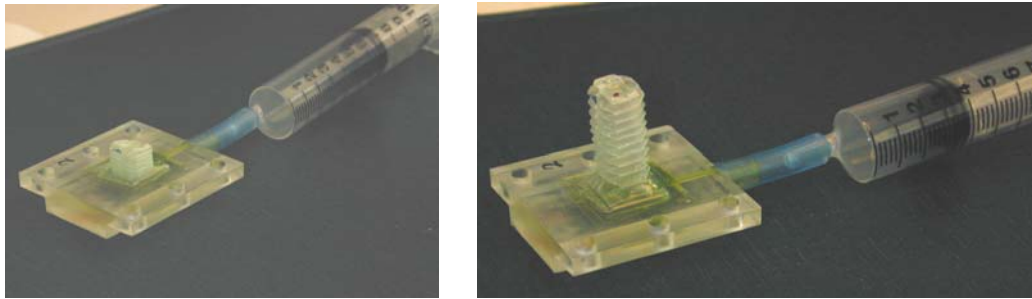
c) Cast sacrificial materials



d) Remove sacrificial after Parylene coating

Figure 31 Fabrication process of bubble actuators

Fig. 31 shows the sequence of the fabrication process for the lantern-shaped angular bubble actuators discussed above. Fabrication process for all three other type bubbles is the same. The sequential process is a) Build corrugated molds by stereo lithography. b) Mold transferring by PDMS. c) Casting sacrificial materials. d) Parylene coating and remove sacrificial materials.



a) Bellows in deflated shape      b) Bellows in inflated shape  
Figure 32 Fluidically-driven bellows

Pictures of the fluidically-driven bellows are shown in Figure 32. a) is in the shrunk shape while b) is in expanded shape.

- **Investigation into MEMS compatible fabrication process for elastomeric materials**

A literature survey of different approaches for MEMS compatible polymers was undertaken. The applicability of dry process such as plasma polymerization and vapor deposition polymerization, and wet process such as dip coating and spray coating have been investigated. Micro dip coating process was selected as an initial method to obtain the corrugated bubbles with large deflection because dip coating can provide a thin shell structure as well as preserve the elastic property of elastomers while others can not assure to maintain elasticity (dry process) after processing or are too difficult to control the thickness and uniformity (spray coating).

Experiments using PDMS have been carried out in dip coating on straight, tapered and corrugated molds in different dimension scales. Free standing PDMS corrugated structures with a thickness of about 100um were obtained. Dip coating on corrugated molds with thin, pre-deposited Parylene was also carried out. Comparison of two bellows bubble structures made by Parylene coating with or without PDMS dip coating is shown in Figure 33. It can be seen that larger restoring force is observed from this “Parylene-PDMS thin film” combined material structure after hyper-expanding two bellows.

Further experiments and characterization will be carried out soon.



a) Hyper expansion of bellows      b) Parylene bellows with(top) or without PDMS layer  
Fig 33. Comparison of Parylene bellows with or without PDMS

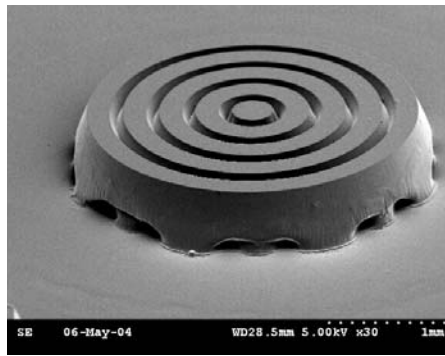
- **MEMS compatible fabrication process of micro-bubble actuators:**

Based on the research of MEMS compatible elastomeric materials and better properties found in combinations of PDMS and Parylene coating structures, a micro-corrugated diaphragm combined with elastic restoring structure has been determined as the whole bubble actuator design. Suitable

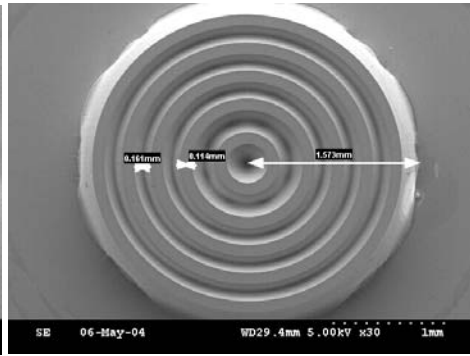
geometries for the corrugated micro-bubble actuators were determined using finite element (FEM) simulation. The simulation also gives directions in selecting the elastomeric materials used for the restoring structure.

The mask was achieved. The main fabrication process using a declined exposure technique has been determined. First prototypes of micro-scale, corrugated SU-8 molds by MEMS compatible process is achieved. SEM pictures of these corrugated micro-molds in different dimension and patterns are shown in Figure 34. The diameter of each mold is about 3 mm, tapered angles are about 15 and 20 degrees.

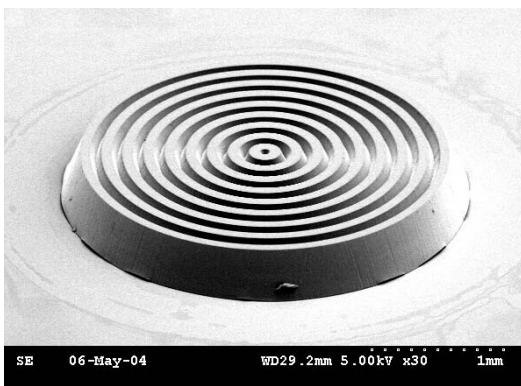
The first prototypes of micro bubble actuators are now being fabricated by MEMS technology.



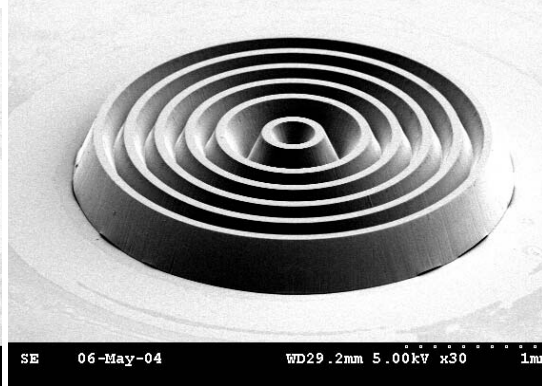
a) Concentric mold with 4 corrugations



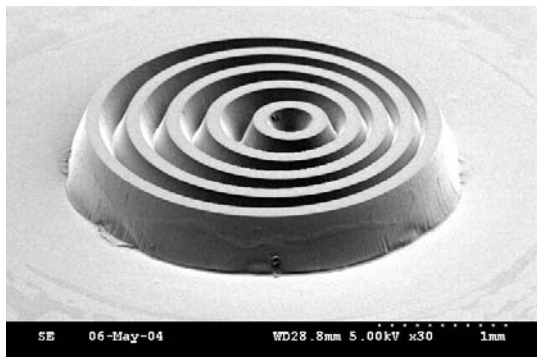
b) Concentric mold with 5 corrugations



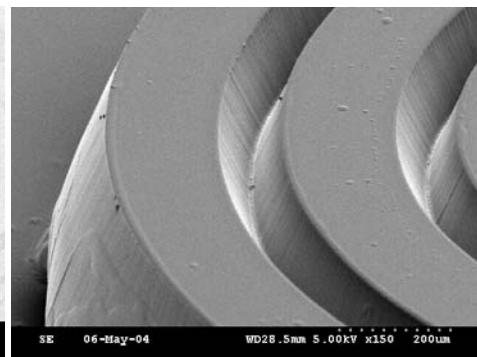
c) Concentric mold with 9 corrugations



d) Concentric mold with 6 corrugations



e) Off center mold with 5 corrugations



f) Enlarged tapered corrugations

Figure 34 SEM pictures of micro corrugated molds by MEMS technology